Exploiting Periodic First-Principles Calculations in NMR Spectroscopy of Disordered Solids

SHARON E. ASHBROOK and DANIEL M. DAWSON*

School of Chemistry and EaStCHEM, University of St Andrews, North Haugh, St Andrews, KY16 9ST UK

Conspectus

Recent advances enabling accurate and efficient determination of Nuclear Magnetic Resonance (NMR) parameters in periodic systems have revolutionized the application of Density Functional Theory (DFT) calculations in solid-state NMR spectroscopy, particularly among experimentalists. Much of the information present in solid-state NMR spectra remains unexploited owing to the difficulty of obtaining high-resolution spectra, and their often challenging assignment. The use of first-principles calculations aids both in the interpretation and assignment of the complex spectral lineshapes observed for solids. Furthermore, for materials with poorly characterized structures calculations provide a method for evaluating potential structural models against experimental data. Determining the structure of well-ordered, periodic crystalline solids can be straightforward using methods exploiting Bragg diffraction. However, it is often the deviations from periodicity, *e.g.*, compositional, positional or temporal disorder, that produce the physical properties (*e.g.,* ferroelectricity or ionic conductivity) that may be of commercial interest. As NMR is sensitive to the atomic-scale environment, it provides a potentially useful tool for studying disordered materials, and the combination of experiment with first-principles calculations offers a particularly attractive approach. In this account we discuss some of the issues associated with the practical implementation of first-principles calculations of NMR parameters in solids, before illustrating the structural insight that can be obtained when such calculations are applied to disordered inorganic materials with two key examples. First, the cation disorder in $Y_2Ti_{2-x}Sn_xO_7$ pyrochlore ceramics (materials proposed as host phases for the encapsulation of lanthanide- and actinide-bearing radioactive waste) is investigated using ^{89}Y and ^{119}Sn NMR. In a second example, ^{17}O NMR is used to probe the dynamic disorder of H in hydroxyl-humite minerals ($n Mg_2SiO_4.Mg(OH)_2$), and ^{19}F NMR is exploited to understand F substitution in these systems. The combined use of first-principles calculations and multinuclear NMR spectroscopy has much to offer for the investigation of local structure, disorder and dynamics in solids, and applications will undoubtedly become more

widespread with future computational and experimental advances. Insight into the atomic-scale environment is a crucial first step in understanding the structure-property relationships in solids, and enabling the efficient design of future materials for a range of ultimate end uses.

Introduction

The wealth of potential information contained within solid-state NMR spectra often cannot be extracted easily or accurately, owing to the anisotropic nature of the interactions influencing the nuclear spins. For powdered solids, broad, featureless lineshapes are typically seen, with limited resolution of distinct species. Despite technological advances providing increases in resolution and sensitivity, the interpretation and assignment of solid-state NMR spectra remains challenging. This is particularly true for inorganic solids, owing to the variety of nuclides studied, the diverse coordination environments and the lack of extensive information (relative to ^{1}H and ^{13}C NMR) in the literature. The recent introduction of the gauge-including projector augmented-wave (GIPAW)[1] approach (utilizing the framework of DFT[2]), enabled NMR parameters to be calculated easily and accurately for periodic solids. This method it is of great interest to theoreticians and experimentalists alike; providing quantitative, theoretical support to relate experimental measurements and atomic-level structure in areas as diverse as biomaterials, minerals, porous frameworks, energy materials and organic solids.[3]

There is a long tradition in the calculation of NMR parameters in quantum chemistry, but predominantly for molecular systems. In this approach, a periodic solid is approximated as a cluster, centered on the atom of interest, with the termination of bonds, usually by H. The accuracy of the calculation increases with cluster size, as does the computational cost and time. For extended structures the termination can lead to significant structural perturbations and, therefore, inaccurate results. The use of a periodic approach, where the three-dimensional structure is recreated from a small-volume unit, enables accurate calculation for all atoms within a system simultaneously.[4] The planewave pseudopotential approach[1] exploits the inherent translational symmetry of solids, enabling the straightforward calculation of NMR parameters including chemical shielding, quadrupolar interactions, scalar couplings and paramagnetic interactions, and has significantly increased the application of such theoretical support among experimentalists.[3] Calculations can be used to interpret and assign high-resolution spectra both

for spin $I = 1/2$ and quadrupolar ($I \geq 1/2$) nuclei, and to provide information that is difficult to extract experimentally (*i.e.*, the relative orientations of tensors), but can significantly influence the appearance of NMR spectra. Calculations can be utilized predictively, guiding experimental acquisition (*e.g.*, the recently-developed Optimization of Pulses Using Structure[5] approach), particularly for challenging systems with poor sensitivity or unknown NMR parameters. For materials with poorly-characterized structures, calculations provide a method for testing structural models against experimental measurements,[3] as exemplified by the recent work by Charpentier and co-workers (combining NMR, DFT and MD) for the study of the structure of silicate glasses.[6] The flexibility and ease with which theoretical structures can be altered provides fundamental insight into the dependence of NMR parameters upon the detailed local geometry.

This account aims to demonstrate how the application of GIPAW calculations has aided the investigation of the atomic-scale environment in disordered inorganic solids using NMR spectroscopy. Structure determination for well-ordered crystalline solids is usually straightforward using Bragg diffraction. However, it is often the deviations in periodicity, *e.g.*, compositional, positional or temporal disorder, that produce the physical properties of commercial interest. The sensitivity of NMR to the atomic-scale environment, and the simultaneous use of DFT calculations to interpret spectra, offers an exciting approach for investigating disordered solids. After a brief discussion of some aspects of the practical implementation of GIPAW DFT calculations, the new insight into disorder and dynamics that the combination of calculation and experiment can provide will be illustrated through examples from recent work.

Practical Aspects of GIPAW Calculations

In DFT the total energy is expressed as a function of the electron density, ρ, enabling a cost-efficient calculation of the ground state electronic structure (and its dependant properties).[2]

Whilst most energetic contributions can be computed exactly, the form of the "exchange-correlation" energy, describing inter-electron interactions, is unknown. Several approximations attempt to account for this, including the local density approximation (LDA),[2] which assumes constant ρ over a small region of space. It is possible to improve accuracy by also considering the gradient of ρ, *i.e.*, gradient generalized approximations (GGA).[2,4] In recent applications of GIPAW calculations to solids, the PBE[7] implementation of GGA has proved a robust, accurate and, consequently, popular approach.

Typically, before DFT calculations of NMR parameters can be used interpretively, it is necessary to evaluate their accuracy (and understand their limitations) for a particular nuclide. This is especially true for inorganic solids that contain a wide range of NMR-active species, about which relatively little (in comparison to ^{1}H and ^{13}C) may be known in the literature. This evaluation is conventionally achieved by a comparison of calculated and measured NMR parameters for a series of crystalline solids with well-characterized structures. Several such investigations have been undertaken recently, including *e.g.*, ^{25}Mg, ^{39}K and ^{71}Ga.[3]

The accuracy of planewave pseudopotential calculations considered here depends upon two variable parameters that are chosen in each calculation; (i) the number of planewaves used, described by a cut-off energy, E_{cut}, and (ii) the number of regularly spaced points (*k*-points) in the Brillouin zone (*i.e.*, the primitive unit cell in reciprocal space) sampled.[4] Ideally, these should be infinitely large – however, the choices are constrained by the hardware and computing time available. It is sufficient to ensure calculations are "converged", *i.e.*, the calculated results do not improve significantly if more planewaves/*k*-points are used.[4] One advantage of such calculations is that it is possible to vary systematically the values of both parameters and observe the effect upon the calculation. An example is shown in Figure 1a, where the calculated ^{29}Si chemical shielding of SiO_2 (coesite) is plotted as a function of E_{cut} with a fixed number of *k*-points. There are significant changes in chemical shielding as E_{cut} is increased initially, but these become smaller for higher values. However, the time (and cost) of the calculation (also plotted in Figure

1a) continues to increase with E_{cut}. The choice of E_{cut} should, therefore, balance accuracy and cost, with 45 Ry appearing optimal here.

Figure 1b shows a comparison of the ^{29}Si calculated isotropic shielding and the corresponding experimental isotropic chemical shielding for a series of simple silicates.[8,9] Good agreement is observed, with linear regression showing that the line of best fit has a gradient close to the ideal value of –1. Such agreement demonstrates that this approach is suitable for the calculation of ^{29}Si chemical shifts, and gives some indication of the accuracy of the results that can be expected (*i.e.*, an average error of ~1% in Figure 1b). For nuclei with $I = 1/2$, such as ^{29}Si, the most commonly calculated parameter is the isotropic shielding, σ_{iso}. Although the anisotropy of the shielding tensor (*i.e.*, its magnitude or "span", Ω (= $\delta_{11} - \delta_{33}$), and shape or "skew", κ (= $3(\delta_{22} - \delta_{iso})/\Omega$) is also calculated, this is often more difficult to measure experimentally when spectra contain multiple distinct resonances (as it is removed by the rapid magic-angle spinning (MAS) used to improve resolution and sensitivity), and only more recently have experiment and calculation been compared.[3] However, for quadrupolar nuclei, the magnitude and asymmetry of the quadrupolar interaction, C_Q and η_Q, respectively, are also excellent probes of local structure and affect the NMR spectra obtained. This is shown in Figure 1c, where ^{17}O lineshapes, extracted for the six distinct sites resolved in a high-resolution MQMAS[10] spectrum of $MgSiO_3$ (orthoenstatite) are compared with lineshapes simulated using parameters calculated using GIPAW.[9] The excellent agreement enables a full assignment of the spectrum, which contradicts a previous literature assignment based on empirical relationships between NMR parameters and the local structure, demonstrating both the success of DFT for calculating NMR parameters in periodic solids and the need to treat earlier results with some caution.

In contrast to experiment, where chemical shifts are quoted relative to a reference value, calculations provide the absolute shielding. The two are related by the relationship

$$\delta_{iso}^{calc} = (\sigma_{ref} - \sigma_{iso}^{calc}) \quad , \qquad (1)$$

where σ_{ref} is the reference shielding. This can be determined by a comparison of calculated shielding and experimental shift for a series of materials, as in Figure 1b, where the y intercept of the line of best fit gives σ_{ref} (here, 312.64 ppm).[8,9]

One crucial consideration when calculating NMR parameters is the availability and accuracy (or otherwise) of a crystal structure or structural model. Structures are often obtained from diffraction experiments, or can be generated computationally. In some cases, *e.g.*, for single-crystal diffraction data, structures may sometimes be used without modification. However, for powder diffraction data, or if lighter atoms have not been located directly but added manually, it may be necessary to "optimize" the geometry before calculation of NMR parameters. In this procedure, the coordinates of some or all of the atoms are varied, in order to minimize the forces upon them. For traditional DFT methods, this often results in an expansion of the unit cell owing, at least partly, to the underestimation of dispersion interactions in the exchange-correlation functional.[2,3] One option is to constrain the unit cell parameters during geometry optimization to those determined by diffraction. While suitable for molecular and ordered solids, this approach is inapplicable to disordered materials where and optimization is vital for obtaining the minimum energy structure.[3,6] The recent introduction of semi-empirical dispersion correction schemes[2,3,11] has provided an alternative option.

Figure 2a shows ^{27}Al and ^{31}P MAS NMR spectra of the calcined aluminophosphate, AlPO-14.[12] The four P species are resolved by ^{31}P MAS NMR, but quadrupolar broadening results in overlapping lineshapes for ^{27}Al (although MQMAS experiments resolve four sites). Spectra simulated using NMR parameters calculated for the crystal structure obtained from powder diffraction are shown in Figure 2a. Poor agreement is observed for both nuclei, with the broader ^{27}Al lineshapes reflecting high C_Q values (5.5 - 10.1 MHz), in contrast to those observed experimentally (2.5 - 4.9 MHz). However, the calculated forces upon the atoms are high, indicating that geometry optimization is required. Figure 2a also shows spectra simulated using NMR parameters calculated after optimization (using the TS[11] dispersion correction scheme).

The agreement with experiment is significantly improved, particularly for the calculated ^{27}Al C_Q values. Furthermore, the changes in the ^{31}P chemical shifts upon optimization change the spectral assignment. Figure 2b shows the alteration of the local structure (Al-O and P-O bond lengths) upon optimization. The typical change in the Al-O distance is ~0.03 Å, although larger changes (0.07–0.1 Å) are observed. The range of Al-O distances is considerably smaller for the optimized structure and similar changes are observed for the P-O distances. The initial and optimized structures would be hard to distinguish by diffraction,[12] but the changes in local structure significantly affect the calculated NMR parameters.

For ordered solids, a periodic approach, recreating the three-dimensional structure from a single unit cell, is efficient and intuitive. However, for disordered materials, where this periodicity is not rigidly retained, periodic boundary conditions limit the possible environments that can be considered in a calculation. In such cases, the aperiodic structure is commonly approximated as a crystal composed of periodically-repeating "supercells".[4] The supercell chosen must be sufficiently large to minimize the effect of the structural variation on the neighboring cells. This approach can be applied to isolated molecules, defects in solids, surfaces and even solutions, in addition to disordered materials.[3]

Finally, it should be noted that whereas NMR experiments are carried out at finite temperature, most DFT calculations are performed at 0 K, *i.e.*, on static structures with no temperature directly included. It is well known that there are many dynamic processes present in solids, which may ultimately limit the accuracy of calculations. However, as NMR is sensitive to dynamics, the differences between calculated and experimental NMR parameters offer insight into the presence and nature of motional processes present.[3,4]

Application to Disordered Solids

Although the comparison of experimental and calculated NMR parameters for simple solids is pre-requisite, the real power of first-principles calculations is their ability to provide insight where structural characterization is more difficult. The vast majority of the information available from solid-state NMR spectra remains unexploited owing to the challenge of obtaining high-resolution spectra, and the difficulty of interpretation and assignment, particularly for disordered materials. First-principles calculations can unlock this untapped potential and provide new information on the atomic-scale environment, as highlighted by the following examples.

Cation disorder in pyrochlore ceramics

The chemical flexibility of oxides with the pyrochlore ($A_2B_2O_7$) structure has generated interest in their utility as hosts for the immobilization of lanthanide- and actinide-bearing nuclear waste.[13] While titanate-based pyrochlores are chemically durable, the incorporation of Sn or Zr increases their tolerance to radiation damage. A detailed insight into local structure and disorder in these materials is vital for understanding their physical and chemical properties, and ultimately for the design of improved wasteforms. The sensitivity of NMR to the atomic-scale environment ensures it is ideally suited for this purpose.

Figure 3a shows ^{89}Y and ^{119}Sn MAS NMR spectra[14-15] of $Y_2Ti_{2-x}Sn_xO_7$, a model solid solution that remains pyrochlore throughout its compositional range, where Y^{3+} (similar charge and size to lanthanides/actinides) provides a direct, non-radioactive probe of the local environment. Although both ^{89}Y and ^{119}Sn have $I = 1/2$ (natural abundances of 100% and 8.6%, respectively), the low gyromagnetic ratio of ^{89}Y and long T_1 relaxation times (often 100-1000 seconds) limit sensitivity and make experimental acquisition considerably more challenging than for ^{119}Sn. In $Y_2Ti_{2-x}Sn_xO_7$, Y occupies the eight-coordinate A site, with Sn/Ti occupying the six-coordinate B site. In both cases the next-nearest neighbour (NNN) environment is similar, with each surrounded by six B sites. The ^{89}Y NMR spectra display numerous spectral resonances,

presumably associated with different numbers and/or arrangements of Sn/Ti occupying the surrounding B sites.[15] However, despite the similar NNN environment, the ^{119}Sn MAS NMR spectra exhibit far fewer resonances, particularly at higher Ti content.[15]

Interpretation of the experimental spectra is facilitated by first-principles calculations, where the effect upon the NMR parameters of a change in the local environment can be investigated easily. When considering B-site substitution, it is impractical to perform calculations on truly disordered solids (as an unfeasibly large number of atoms would be involved), and a simplified approach is required.[16] The local environment of one Y (or Sn) cation within the unit cell is systematically varied to include all possible combinations of Sn/Ti on the six surrounding B sites, as shown in Figure 3b.[16] Structures are optimized and NMR parameters calculated for all Y (or Sn) within the cell. Calculated (^{89}Y and ^{119}Sn) chemical shifts[15,16] are shown in Figure 3c, with the number and spatial arrangement of Sn NNN (*n*) indicated. For ^{89}Y, there is a systematic increase of ~20 ppm in the average chemical shift as Sn is substituted onto the NNN B sites, a change of similar magnitude to the spacing of the spectral resonances. For any *n* Sn NNN, however, a similar range of chemical shifts is predicted for the different spatial arrangements of Sn/Ti. This suggests that the different ^{89}Y resonances resolved experimentally result from different *n* Sn NNN, and that the broadening, splittings and shoulders present reflect the different spatial arrangements of these neighbours and longer-range structural changes. In contrast, a small change in the average ^{119}Sn chemical shift is observed with the introduction of Ti into Sn-rich NNN environments;[15] however, this change reduces as the Ti content of the surrounding B sites increases, resulting in overlap of the calculated chemical shifts. This agrees with the experimental NMR spectra in Figure 3a, where broad, overlapped resonances are observed. Further DFT calculations reveal two opposing contributions to the ^{119}Sn chemical shift; an upfield shift produced by the substitution of Ti into the NNN environment, and a concomitant downfield shift arising from the change in unit cell size upon substitution of the smaller cation.[15]

Although these contributions are also present for ^{89}Y, the former is considerably larger than the latter, resulting in well-resolved spectral resonances.[16]

Although DFT provides a general understanding of the spectral appearance (and a tentative assignment for ^{89}Y), there remains some need for caution. Owing to the range of calculated shifts for each environment, some resonances with similar shifts are assigned to differing NNN environments, and others with very different shifts are attributed to the same NNN environment. Confidence in the assignment can be improved by considering an additional probe of the local environment – *e.g.*, the span of the shielding anisotropy (Ω). Although a sensitive probe of structure, the shielding anisotropy is removed under the rapid MAS used to improve spectral resolution and sensitivity. Information can be obtained from slow MAS spectra, but for systems containing multiple environments, overlapping sideband manifolds can lead to difficulties in extracting accurate information. A number of two-dimensional methods have been proposed to overcome this, where fast MAS affords high resolution, but the anisotropic interaction is "recoupled" in a second dimension, producing a sideband manifold that can be analyzed. "Amplification" of the interaction, enabling the accurate measurement of smaller anisotropies (*e.g.*, the CSA-amplified PASS experiment), is also possible.[17,18] These approaches, originally implemented for ^{13}C and ^{31}P, have recently been extended to ^{89}Y, with appropriate modification of the experimental pulse sequence and the fitting procedures employed.[19]

Figure 4a shows an ^{89}Y CSA-amplified PASS spectrum of $Y_2Ti_{0.4}Sn_{1.6}O_7$,[19] acquired in a total experimental time of ~12.5 days (highlighting the challenges of ^{89}Y NMR for disordered materials). For each resonance, values of Ω, (and κ) can be measured from the sideband manifold. The contour plots, also in Figure 4a show the root-mean-square (rms) error associated with fits for varying values of Ω (and κ), and provide information on the "best fit" and associated confidence limits. The experimentally-measured values of Ω can be compared to those calculated as described above.[19] Figure 4b summarizes the variation in both the calculated isotropic and anisotropic shielding with the NNN environment, with a significant change in Ω

(of ~80 ppm) observed as Sn/Ti is substituted onto the surrounding B sites. Figure 4b also plots experimental measurements (in this case for $Y_2Ti_{0.8}Sn_{1.2}O_7$), demonstrating that spectral assignment is considerably eased by considering two parameters simultaneously. With the assignment complete, insight into the distribution of Sn/Ti is gained by comparing the relative spectral intensities to the probability of finding a particular number of Sn/Ti NNN.[15,19] The best match indicates randomly distributed Sn/Ti, with no evidence for clustering or ordering of the B-site cations. Furthermore, it is possible to correlate changes in Ω directly to the detailed local structure, as shown in Figure 4c, where the dependence upon the (average) Y-O_{8b} bond distance is plotted. A strong, almost linear, correlation (of *ca.* −109 ppm/0.02 Å) is observed, enabling the estimation of such distances for the differing environments in disordered $Y_2Ti_{2-x}Sn_xO_7$ pyrochlores.[19]

The combination of high-resolution NMR and GIPAW DFT calculations enables detailed information to be obtained about the nature of the B-site cation disorder in pyrochlores and provides detailed insight into the local geometry - information it is difficult to obtain from diffraction-based methods. Such an approach offers great potential for future application in this area, particularly for understanding the more complex ceramic phases of interest in waste encapsulation.

Disorder in hydrous silicates

The Earth's mantle contains an estimated 200-500 ppm hydrogen (often termer "water"),[20] although little is known about its exact mechanism of incorporation into the structures of the nominally-anhydrous inner-Earth minerals. As the structural chemistry of low levels of hydrogen is difficult to determine by diffraction, NMR spectroscopy offers a useful alternative approach. The dominant mineral in the Earth's upper mantle is olivine (α-$Mg_{1.8}Fe_{0.2}SiO_4$). The minerals in the hydroxyl-humite group, $n Mg_2SiO_4.Mg(OH)_2$, have been proposed as models of

the defect sites that occur when water is incorporated into olivine, as their structures can be viewed as consisting of *n* layers of forsterite (the Mg end-member of the α-$Mg_{2-x}Fe_xSiO_4$ solid solution) alternating with layers of $Mg(OH)_2$.[21] Diffraction studies of clinohumite (n = 4) have revealed two distinct H sites (H1 and H2) for each hydroxyl group, each with 50% occupancy, indicating the disordered nature of the minerals.[21]

A high-resolution isotropic ^{17}O (9.4 T) NMR spectrum of clinohumite, obtained from a MQMAS experiment, is shown in Figure 5a.[22] Five resonances are resolved, although their relative intensities (2:2:2:1:1) suggest that all eight silicate oxygens are observed. (Note the hydroxyl oxygen (O9) is not observed at this magnetic field strength and MAS rate, owing to its large C_Q). A tentative assignment of the spectrum can be made by comparison to spectra of chondrodite and forsterite (not shown).[22] Figure 5a also shows an ^{17}O isotropic spectrum, simulated using NMR parameters from GIPAW DFT calculations.[23] These were carried out for a series of model structures, with differing positions of the hydroxyl groups within the unit cell, and the results from each calculation summed together, to model the disordered mineral. There is poor agreement between calculation and experiment, with many more resonances observed in the calculated spectra, indicating that the NMR parameters are sensitive to the exact hydroxyl positions. However, if the calculated NMR parameters of each oxygen species in each of the structural models are averaged, the simulated spectrum (also shown in Figure 5a) agrees much better with experiment,[23] suggesting that there is dynamic, rather than static, disorder of the hydroxyl groups, resulting in a full averaging of the NMR parameters. The simulated spectrum also shows that the previous assignment of O7 and O3 must be reversed.

The presence of dynamics in clinohumite is supported by the isotopic spectrum obtained from STMAS[24] (an alternative to MQMAS for removing quadrupolar broadening), where a significant broadening of some of the resonances is observed (Figure 5b).[23] STMAS spectra are sensitive to μs-timescale dynamics,[25] owing to the use of satellite transitions within the experiment. The broadening observed depends upon the change in the quadrupolar interaction

during the motional process and the timescale of this change. As the first of these can be determined using the calculations described above (if the magnitude, asymmetry and relative orientation of the quadrupole tensor for each oxygen species in all possible model structures is known), the latter can, therefore, also be established (using a simple model for motional broadening[26]). Figure 5b also shows ^{17}O STMAS isotropic spectra simulated using the calculated NMR parameters for different motional rates.[23] Despite the simplicity of the models used, good agreement between experiment and calculation is obtained when $\log_{10}k = 5.5$ (*i.e.*, $k \approx 3.2 \times 10^5$ s^{-1}). This measurement is supported by ^{2}H MAS NMR (not shown)[27] of deuterated clinohumite, where the temperature-dependent linewidth allows an activation energy of 40 ± 4 kJ mol^{-1} for H1/H2 exchange to be determined.[27]

Many natural humite minerals exist with significant levels of fluorine substitution. Diffraction studies of fluorine-rich clinohumite show a single hydrogen site arising from the formation of OH…F hydrogen bonds, which inhibits H1/H2 exchange. Although this indicates some degree of local order, the positions of F^- and OH^- are not distinguished by diffraction.[28] However, a ^{19}F MAS NMR spectrum of (54%) fluorinated clinohumite, shown in Figure 6a, reveals four distinct F environments, indicating a more disordered material than previously thought.[29] GIPAW DFT calculations (using supercells with differing levels and positions of F substitution) reveal four ranges of chemical shifts, in agreement with the experimental resonance positions, as shown in Figure 6a.[29] The calculations reveal that the ^{19}F chemical shift is sensitive to the nature of the nearby anions (*i.e.*, F^- or OH^-) - the two closest are at 2.7 and 3.2 Å. The assignment of the spectral resonances can be confirmed using two-dimensional correlation spectra, *e.g.*, as shown in Figure 6b, where pairs of peaks either side of the diagonal indicate two F in close spatial proximity (as transfer is through the dipolar coupling).[29]

Similar two-dimensional spectra, using transfer *via* the *J* coupling,[29] can also be obtained. The magnitude of these *J* couplings can be determined from the lineshapes in the *J*-resolved spectrum, as shown in Figure 6c.[29] No couplings are observed for F_A (surrounded by OH^-

groups), while couplings of ~3-4 Hz and ~18-19 Hz are observed for F_B and F_C, respectively. For F_D both small and larger couplings are apparent. There are two possible "through-bond" pathways between adjacent F species (F-Mg-F' and F-Mg-O-Mg-F', respectively), perhaps accounting for two different couplings; however, the F-Mg interaction is expected to be mostly ionic in character. Previously "through-space" *J* couplings between F atoms in close spatial proximity but not formally chemically bonded, have been observed previously in organofluorine compounds.[30] This interaction is thought to be *via* direct overlap of fluorine lone pairs. The distance between adjacent fluorines in clinohumite is similar to the sum of the ionic radii suggesting that there may be a significant through-space component to the *J* coupling. Some insight can be obtained from calculations carried out for a $3 \times 1 \times 1$ supercell of fully-fluorinated clinohumite, where couplings between adjacent ^{19}F of ~3.5 and 12 Hz are found, as shown in Figure 6d.[29]Although perfect agreement between experiment and calculation is impossible owing to the simplified nature of the model, the calculated values agree qualitatively with experiment. It is also noticeable that, as shown in Figure 6d, there are two possible interactions between F with similar "through-bond" (*i.e.*, $^4J_{FF}$) pathways but differing distances (3.18 Å and 4.77 Å, respectively). However, significant *J* couplings are only calculated between the two closest F species, confirming the through-space character of the interaction.

Once assigned, the relative intensities of the ^{19}F resonances provide insight into the anion disorder in fluorinated humites. The NMR spectra reveal that although the formation of OH…F hydrogen bonds appears favorable, these minerals are significantly disordered, with F-rich and OH-rich regions present. Only the H1 site is occupied when hydrogen bonds are formed, whereas H1 and H2 are both occupied (and in dynamic exchange) in the OH-rich regions.[29]

Summary

Recent advances enabling accurate and efficient determination of NMR parameters in periodic systems have revolutionized the application of DFT calculations in solid-state NMR spectroscopy. Calculations can be used to assign high-resolution spectra and, for more complex materials, such as those discussed here, aid spectral interpretation and provide insight into the atomic-scale structure and disorder. The increasing availability of large computing facilities is enabling the study of larger, more complicated systems, while developments in processor technology continue to increase calculation efficiency. These improvements will ease the investigation of disordered materials in the future. Anticipated software developments, *e.g.*, the more widespread incorporation of dispersion forces, relativistic effects and paramagnetic interactions into available codes, will improve the scope and accuracy of calculations. In general, NMR spectroscopy, with its sensitivity to local structure, offers a complementary tool to diffraction for obtaining a complete picture of solid-state structures. DFT calculations connect these techniques, enabling confirmation, adaption or refinement of structural models, and providing more detailed local information. This combined approach is becoming more widespread and rapid progress is anticipated in the coming years, with the ultimate goal of understanding structure-property relationships in solids, enabling materials to be "designed" for specific applications.

Biographical Information

Sharon Ashbrook (b. 1975) graduated with an MChem from Hertford College, Oxford, in 1997, before studying for her DPhil (2001) in Oxford in the group of Professor Stephen Wimperis. In 2003, she was awarded a Royal Society Dorothy Hodgkin Fellowship, which she held at the Department of Earth Sciences, Cambridge and, subsequently, in St Andrews. She also held the Charles and Katherine Darwin Research Fellowship at Darwin College, Cambridge. From 2005, she was appointed as an RCUK Academic Fellow in the School of Chemistry at the

University of St Andrews, and was promoted to Reader in 2009. Her research focuses on the application of multinuclear solid-state NMR techniques, and their combination with first-principles DFT calculations, to investigate structure, disorder and dynamics in inorganic solids, and she has published ~100 papers in this area. She was awarded the RSC Harrison Prize in 2004, the RSC Marlow Award for Physical Chemistry in 2011, and the RSE Makdougall Brisbane Medal for Physical Science in 2012.

Daniel Dawson (b. 1987) obtained an MChem from the University of Liverpool in 2009 and is currently studying for a PhD in the group of Sharon Ashbrook. His work is focused on understanding microporous materials through a combination of solid-state NMR spectroscopy and DFT calculations.

References

1. Pickard, C. J.; Mauri, F. All-electron magnetic response with pseudopotentials: NMR chemical shifts. *Phys. Rev. B* **2001**, *63*, 245101.

2. Martin, R. M. Electronic structure: Basic theory and practical methods, CUP, Cambridge, **2004**.

3. C. Bonhomme, C. Gervais, F. Babonneau, C. Coelho, F. Pourpoint, T. Azaïs, S. E. Ashbrook, J. M. Griffin, J. R. Yates, F. Mauri, and C. J. Pickard, First-Principles Calculation of NMR Parameters Using the GIPAW (Gauge Including Projector Augmented Wave) Method: a Chemistry Point of View, *Chem. Rev.* **2012**, *112*, 5733-5779.

4. Yates, J. R.; Pickard, C. J. Computations of magnetic resonance parameters for crystalline systems: principles, in "Encyclopedia of Magnetic Resonance", Wiley **2008**.

5. O'Dell, L. A; Ratcliffe, C. I. Crystal Structure Based Design of Signal Enhancement Schemes for Solid-State NMR of Insensitive Half-Integer Quadrupolar Nuclei, *J. Phys. Chem. A* **2011**, *115*, 747-752.

6. Charpentier, T.; Ispas, S.; Profeta, M.; Pickard, C. J. First-principles calculation of O-17, Si-29, and Na-23 NMR spectra of sodium silicate crystals and glasses, J. Phys. Chem. B **2004**, *108*, 4147-4161.

7. Perdew, J. P.; Burke, K.; Ernzerhof, M. Generalized Gradient Approximation made simple, *Phys. Rev. Lett.* **1996**, *77*, 3865-3868.

8. Ashbrook, S. E.; Le Polles, L.; Pickard, C. J.; Berry, A. J.; Wimperis, S.; Farnan, I. First-principles calculations of solid-state ^{17}O and ^{29}Si NMR spectra of Mg_2SiO_4 polymorphs, *Phys. Chem. Chem. Phys.* **2007**, *9*, 1587-1598.

9. Ashbrook, S. E.; Berry, A. J.; Frost, D. J.; Gregorovic, A.; Pickard, C. J.; Readman, J. E.; Wimperis, S. ^{17}O and ^{29}Si NMR parameters of $MgSiO_3$ phases from high-resolution solid-state NMR spectroscopy and first-principles calculations, *J. Am. Chem. Soc.* **2007**, *129*, 13213-13224.

10. Frydman, L.; Harwood, J. S. Isotropic spectra of half-integer quadrupolar spins from bidimensional magic-angle spinning NMR, *J. Am. Chem. Soc.* **1995**, *117*, 5367-5368.

11. Tkatchenko, A.; Scheffler, M. Accurate molecular van der Waals interactions from ground-state electron density and free-atom reference data, *Phys. Rev. Lett.* **2009**, 102, 073005.

12. Ashbrook, S. E.; Cutajar, M.; Pickard, C. J.; Walton, R. I.; Wimperis, S. Structure and NMR assignment in calcined and as-synthesized forms of AlPO-14: a combined study by first-principles calculations and high-resolution ^{27}Al–^{31}P MAS NMR correlation, *Phys. Chem. Chem. Phys.* **2008**, *10*, 5754-5767.

13. Ewing, R. C.; Weber, W. J.; Lian, J. Nuclear waste disposal—pyrochlore ($A_2B_2O_7$): Nuclear wasteform for the immobilization of plutonium and ''minor'' actinides, *Appl. Phys. Rev.* **2004**, *95*, 5949-5971.

14. Ashbrook, S. E.; Whittle, K. R.; Lumpkin, G. R.; Farnan, I. ^{89}Y magic-angle spinning NMR of $Y_2Ti_{2-x}Sn_xO_7$ pyrochlores, *J. Phys. Chem. B* **2006**, *110*, 10358-10364.

15. Mitchell, M. R.; Reader, S. W.; Johnston, K. E.; Pickard, C. J.; Whittle, K. R.; Ashbrook, S. E. ^{119}Sn MAS NMR and first-principles calculations for the investigation of disorder in stannate pyrochlores, *Phys. Chem. Chem. Phys.* **2011**, *13*, 488-497.

16. Reader, S. W.; Mitchell, M. R.; Johnston, K. E.; Pickard, C. J.; Whittle, K. R.; Ashbrook, S. E. Cation disorder in pyrochlore ceramics: ^{89}Y MAS NMR and first-principles calculations, *J. Phys. Chem. C* **2009**, *113*, 18874-18883.

17. Shao, L.; Titman, J. J. Chemical shift anisotropy amplification, *Prog. NMR Spectrosc.* **2007**, *51*, 103-137.

18. Orr, R. M.; Duer, M. J.; Ashbrook, S. E. Correlating fast and slow chemical shift spinning sideband patterns in solid-state NMR, *J. Magn. Reson.* **2005**, *174*, 301-309.

19. Mitchell, M. R.; Carnevale, D.; Orr, R.; Whittle, K. R.; Ashbrook, S. E. Exploiting the chemical shielding anisotropy to probe structure and disorder in ceramics: ^{89}Y MAS NMR and first-principles calculations, *J. Phys. Chem. C* **2012**, *116,* 4273-4286.

20. Bell, D. R.; Rossman, G. R. Water in the Earth's mantle; the role of nominally anhydrous minerals, *Science* **1992**, *255*, 1391-1397.

21. Berry, A. J.; James, M. Refinement of hydrogen positions in synthetic hydroxyl-clinohumite by powder neutron diffraction, *Am. Mineral.* **2001**, *86*, 181-184.

22. Ashbrook, S. E.; Berry, A. J.; Wimperis, S. ^{17}O Multiple-quantum MAS NMR study of high-pressure hydrous magnesium silicates, *J. Am. Chem. Soc.* **2001**, *123*, 6360-6366.

23. Griffin, J. M.; Wimperis, S.; Berry, A. J.; Pickard, C. J.; E. Ashbrook, S. E. Solid-state ^{17}O NMR spectroscopy of hydrous magnesium silicates: Evidence for proton dynamics, *J. Phys. Chem. C* **2009**, *113*, 465-471.

24. Ashbrook, S. E.; Wimperis, S. High-resolution NMR of quadrupolar nuclei in solids: the satellite-transition magic-angle spinning (STMAS) experiment, *Prog. NMR Spectrosc.* **2004**, *45*, 53-108.

25. Antonijevic, S.; Ashbrook, S. E.; Biedasek, S.; Walton, R. I.; Wimperis, S.; Yang, H. X. Dynamics on the microsecond timescale in microporous aluminophosphate AlPO-14 as evidenced by ^{27}Al MQMAS and STMAS NMR Spectroscopy, *J. Am. Chem. Soc.* **2006**, *128*, 8054-8062.

26. Cutajar, M.; Ashbrook. S. E.; Wimperis, S. ^{2}H Double-quantum MAS NMR spectroscopy as a probe of dynamics on the microsecond timescale in solids, *Chem. Phys. Lett.* **2006**, *423*, 276-281.

27. Griffin, J. M.; Miller, A. J.; Berry, A. J.; Wimperis, S.; Ashbrook, S. E. Dynamics on the microsecond timescale in hydrous silicates studied by solid-state ^{2}H NMR spectroscopy, *Phys. Chem. Chem. Phys.* **2010**, *12*, 2989-2998.

28. Friedrich, A.; Lager, G. A.; Ulmer, P.; Kunz, M.; Marshall, W. G. High-pressure single-crystal X-ray and powder neutron study of F,OH/OD-chondrodite: Compressibility, structure, and hydrogen bonding, *Am. Mineral.* **2002**, *87*, 931-939.

29. Griffin, J. M.; Yates, J. R.; Berry, A. J.; Wimperis, S.; Ashbrook, S. E. High-resolution ^{19}F MAS NMR spectroscopy: Structural disorder and unusual *J* couplings in a fluorinated hydroxy-silicate, *J. Am. Chem. Soc.* **2010**, *132*, 15651-15660.

30. Mallory, F. B.; *et al*. Nuclear spin-spin coupling via nonbonded interactions. *J. Am. Chem. Soc.* **2000**, *122*, 4108-4116.

Figure 1. (a) Plot showing the ^{29}Si calculated isotropic shielding of SiO_2 coesite as a function of the planewave cut-off energy, E_{cut}. The computational time is also shown. (b) Comparison of ^{29}Si calculated isotropic shielding and experimental isotropic shifts for a series of silicates. (c) Comparison of experimental quadrupolar lineshapes extracted from an ^{17}O MQMAS NMR spectrum of $MgSiO_3$, with those simulated using NMR parameters calculated by DFT. Adapted from Ref. 9.

Figure 2. (a) Experimental (14.1 T) ^{27}Al and ^{31}P MAS NMR spectra for calcined AlPO-14, and lineshapes simulated using the NMR parameters calculated using DFT prior to and post structural optimization. (b) Plot of Al-O and P-O bond distances for calcined AlPO-14 prior to and post structural optimization.

Figure 3. (a) ^{89}Y and ^{119}Sn (14.1 T) MAS NMR spectra of $Y_2Ti_{2-x}Sn_xO_7$ pyrochlores. (b) Possible arrangements of Sn/Ti on the six NNN B sites that surround both A and B cation sites. (c) Plots showing the calculated ^{89}Y and ^{119}Sn isotropic chemical shifts as a function of the number of Sn NNN. Reprinted with permission from *J. Phys. Chem. C* **2009**, *113*, 18874. Copyright 2009 American Chemical Society and reproduced (in part) from Ref. [15] with permission of the PCCP Owner Societies.

Figure 4. (a) ^{89}Y (14.1 T) CSA-amplified PASS spectrum of $Y_2Ti_{0.4}Sn_{1.6}O_7$, acquired in a total experiment time of ~12.5 days, with contour plots showing the rms deviation from analytical fitting of each sideband manifold for varying Ω and κ. (b) Plot showing the calculated ^{89}Y shielding parameters (isotropic shift and span) for disordered pyrochlore model structures. Overlaid are ^{89}Y experimental measurements for $Y_2Ti_{0.8}Sn_{1.2}O_7$. (c) Plot showing the dependence of the calculated ^{89}Y span on the (average) $Y–O_{8b}$ bond distance. Reprinted with permission from *J. Phys. Chem. C* **2012**, *116*, 4273-4286. Copyright 2012 American Chemical Society.

Figure 5. ^{17}O (9.4 T) isotropic (a) MQMAS and (b) STMAS spectra of clinohumite ($4Mg_2SiO_4.Mg(OH)_2$). Also shown in (a), are spectra resulting from the summation and averaging of simulated ^{17}O isotropic spectra calculated for different possible arrangements of the hydroxyl groups. In (b), STMAS spectra are simulated using the calculated NMR parameters for the different structural models, and an additional line broadening determined using a simple model for motional broadening. Adapted from Ref. 23.

Figure 6. ^{19}F (a) MAS, (b) through-space DQMAS and (c) ^{19}F *J*-resolved NMR spectra of (54%) fluorinated clinohumite ($4Mg_2SiO_4.Mg(OH,F)_2$). In (a), calculated chemical for model structures with varying amounts and positions of F substitution are shown. (d) An expanded view of the structure of fully-fluorinated clinohumite, showing distances between adjacent fluorine sites and calculated *J* couplings. Reprinted with permission from *J. Am. Chem. Soc.* **2010**, *132*, 15651-15660. Copyright 2010 American Chemical Society.

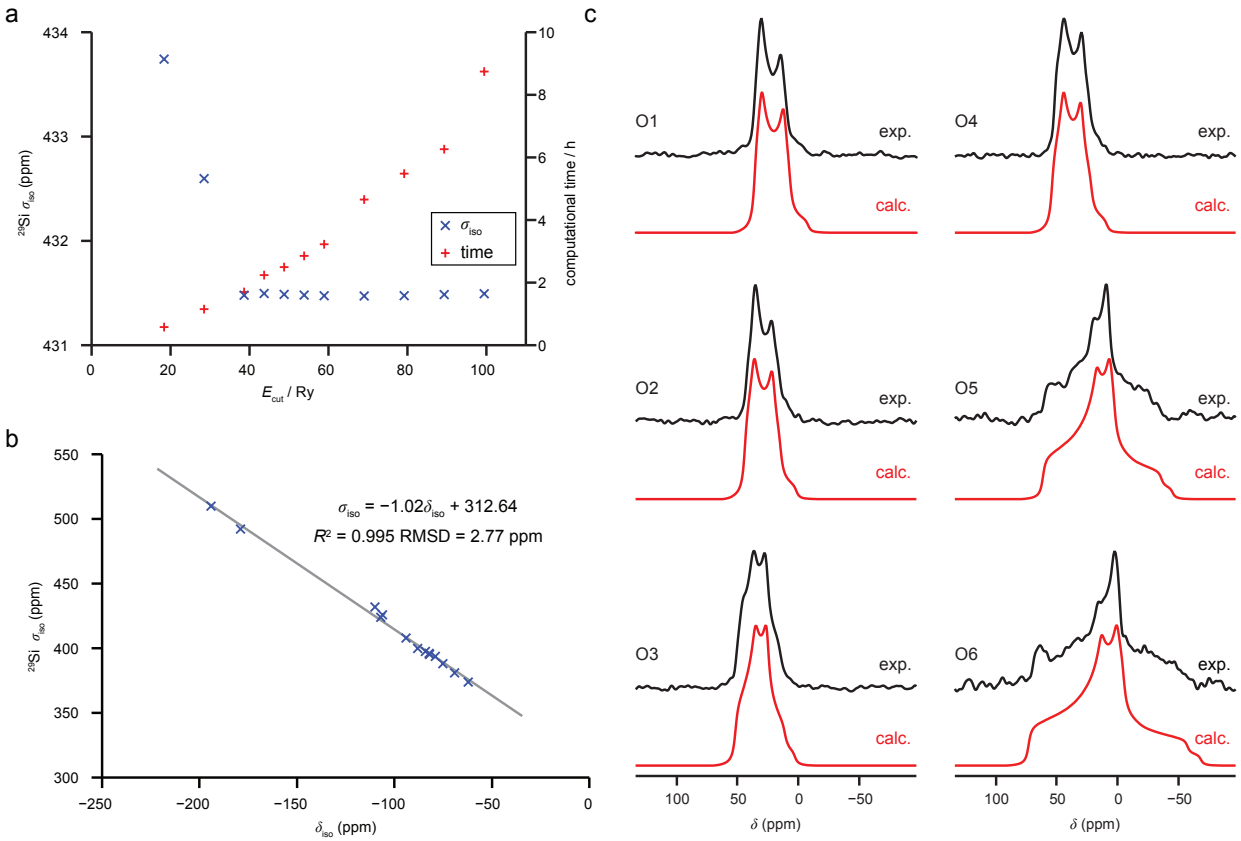
a
b
c
^{29}Si σ_{iso} (ppm)
computational time / h
E_{cut} / Ry
σ_{iso}
time
σ_{iso} = −1.02δ_{iso} + 312.64
R^2 = 0.995 RMSD = 2.77 ppm
δ_{iso} (ppm)
O1
O2
O3
O4
O5
O6
exp.
calc.
δ (ppm)

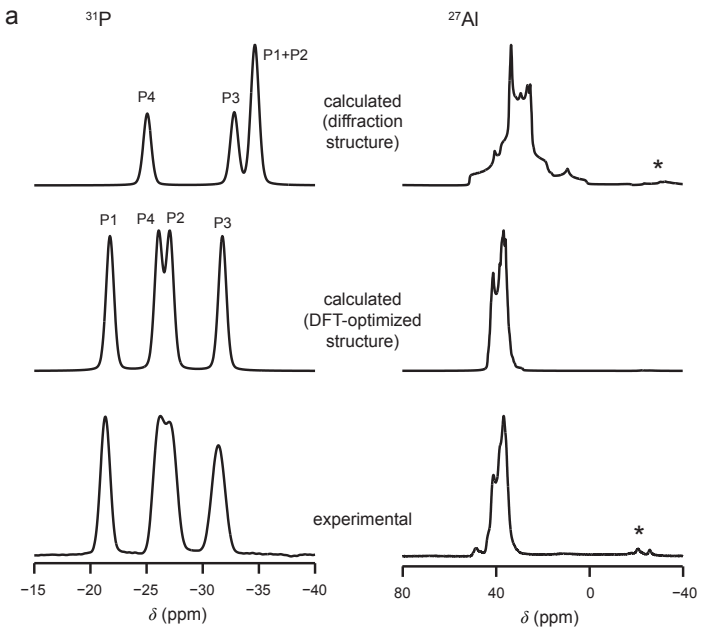
a
31P
27Al
P1+P2
P4
P3
calculated
(diffraction
structure)
P1
P4
P2
P3
calculated
(DFT-optimized
structure)
experimental
*
*
−15
−20
−25
−30
−35
−40
δ (ppm)
80
40
0
−40
δ (ppm)

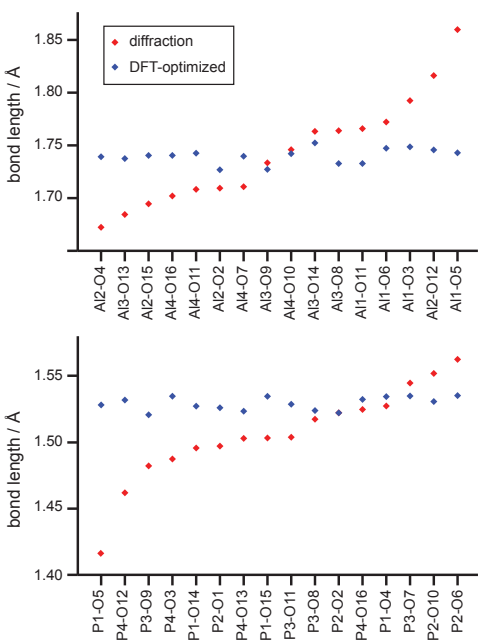
b
diffraction
DFT-optimized
bond length / Å
1.85
1.80
1.75
1.70
Al2-O4
Al3-O13
Al2-O15
Al4-O16
Al4-O11
Al2-O2
Al4-O7
Al3-O9
Al4-O10
Al3-O14
Al3-O8
Al1-O11
Al1-O6
Al1-O3
Al2-O12
Al1-O5
bond length / Å
1.55
1.50
1.45
1.40
P1-O5
P4-O12
P3-O9
P4-O3
P1-O14
P2-O1
P4-O13
P1-O15
P3-O11
P3-O8
P2-O2
P4-O16
P1-O4
P3-O7
P2-O10
P2-O6

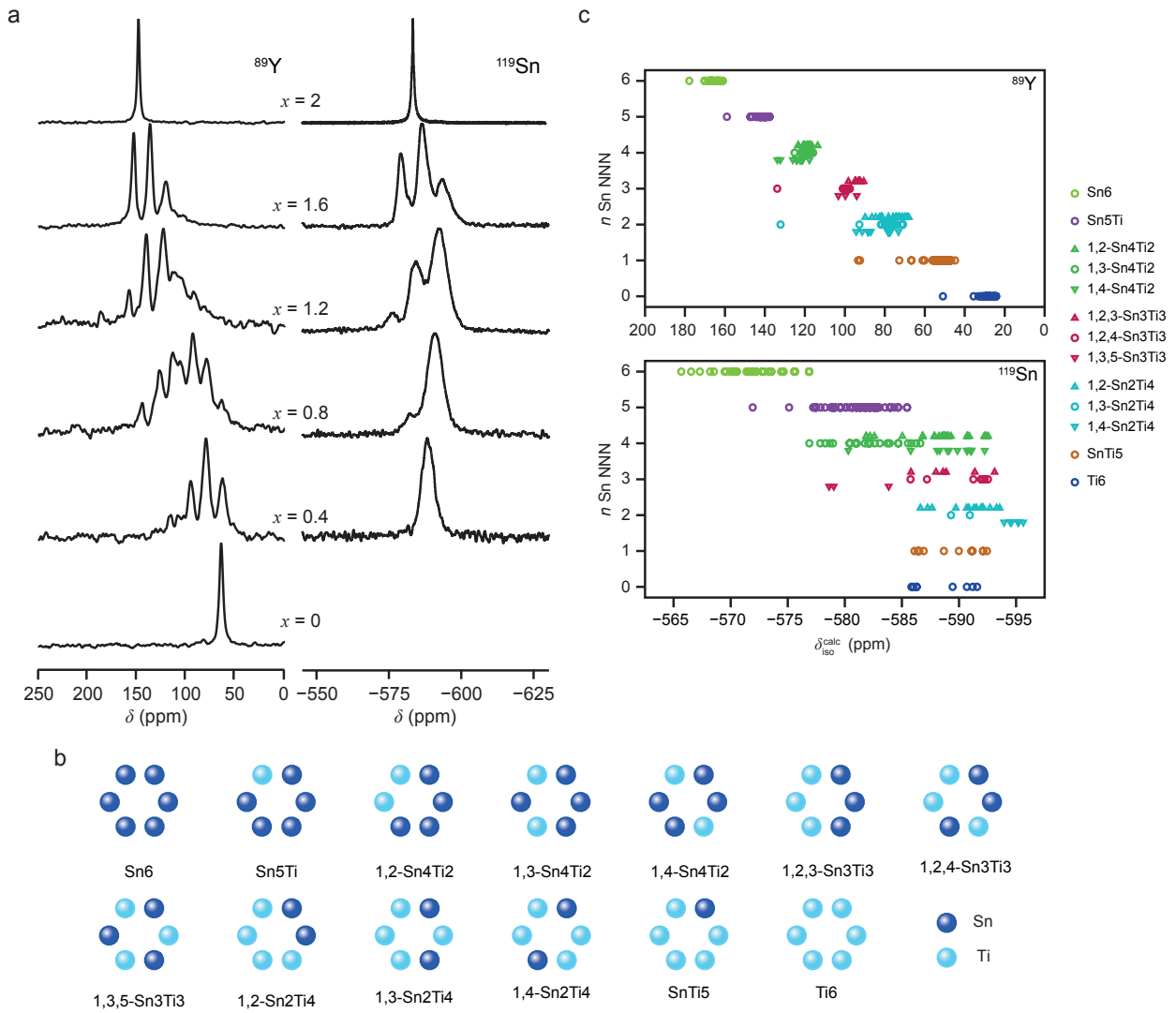
a
89Y
119Sn
x = 2
x = 1.6
x = 1.2
x = 0.8
x = 0.4
x = 0
250 200 150 100 50 0
−550 −575 −600 −625
δ (ppm)
δ (ppm)
c
89Y
119Sn
n Sn NNN
200 180 160 140 120 100 80 60 40 20 0
−565 −570 −575 −580 −585 −590 −595
δ calc iso (ppm)
Sn6
Sn5Ti
1,2-Sn4Ti2
1,3-Sn4Ti2
1,4-Sn4Ti2
1,2,3-Sn3Ti3
1,2,4-Sn3Ti3
1,3,5-Sn3Ti3
1,2-Sn2Ti4
1,3-Sn2Ti4
1,4-Sn2Ti4
SnTi5
Ti6
b
Sn6
Sn5Ti
1,2-Sn4Ti2
1,3-Sn4Ti2
1,4-Sn4Ti2
1,2,3-Sn3Ti3
1,2,4-Sn3Ti3
1,3,5-Sn3Ti3
1,2-Sn2Ti4
1,3-Sn2Ti4
1,4-Sn2Ti4
SnTi5
Ti6
Sn
Ti

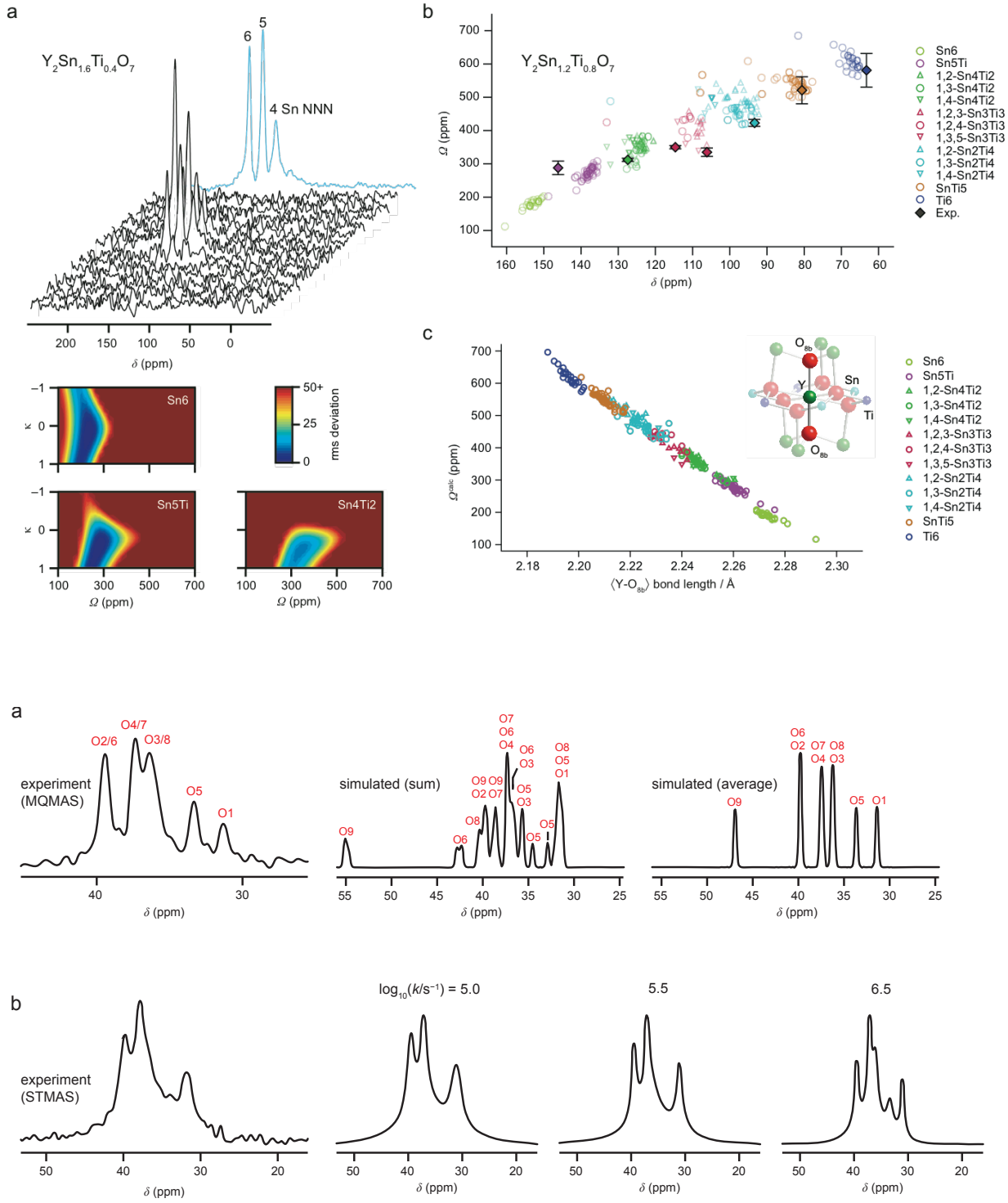
a
$Y_2Sn_{1.6}Ti_{0.4}O_7$
6
5
4 Sn NNN
200 150 100 50 0
δ (ppm)
Sn6
Sn5Ti
Sn4Ti2
κ
Ω (ppm)
50+
25
0
rms deviation
b
$Y_2Sn_{1.2}Ti_{0.8}O_7$
Ω (ppm)
δ (ppm)
Sn6
Sn5Ti
1,2-Sn4Ti2
1,3-Sn4Ti2
1,4-Sn4Ti2
1,2,3-Sn3Ti3
1,2,4-Sn3Ti3
1,3,5-Sn3Ti3
1,2-Sn2Ti4
1,3-Sn2Ti4
1,4-Sn2Ti4
SnTi5
Ti6
Exp.
c
Ω^{calc} (ppm)
⟨Y-O8b⟩ bond length / Å
O8b
Y
Sn
Ti
Sn6
Sn5Ti
1,2-Sn4Ti2
1,3-Sn4Ti2
1,4-Sn4Ti2
1,2,3-Sn3Ti3
1,2,4-Sn3Ti3
1,3,5-Sn3Ti3
1,2-Sn2Ti4
1,3-Sn2Ti4
1,4-Sn2Ti4
SnTi5
Ti6

a
experiment (MQMAS)
O2/6
O4/7
O3/8
O5
O1
simulated (sum)
simulated (average)
δ (ppm)
b
experiment (STMAS)
$\log_{10}(k/s^{-1})$ = 5.0
5.5
6.5
δ (ppm)

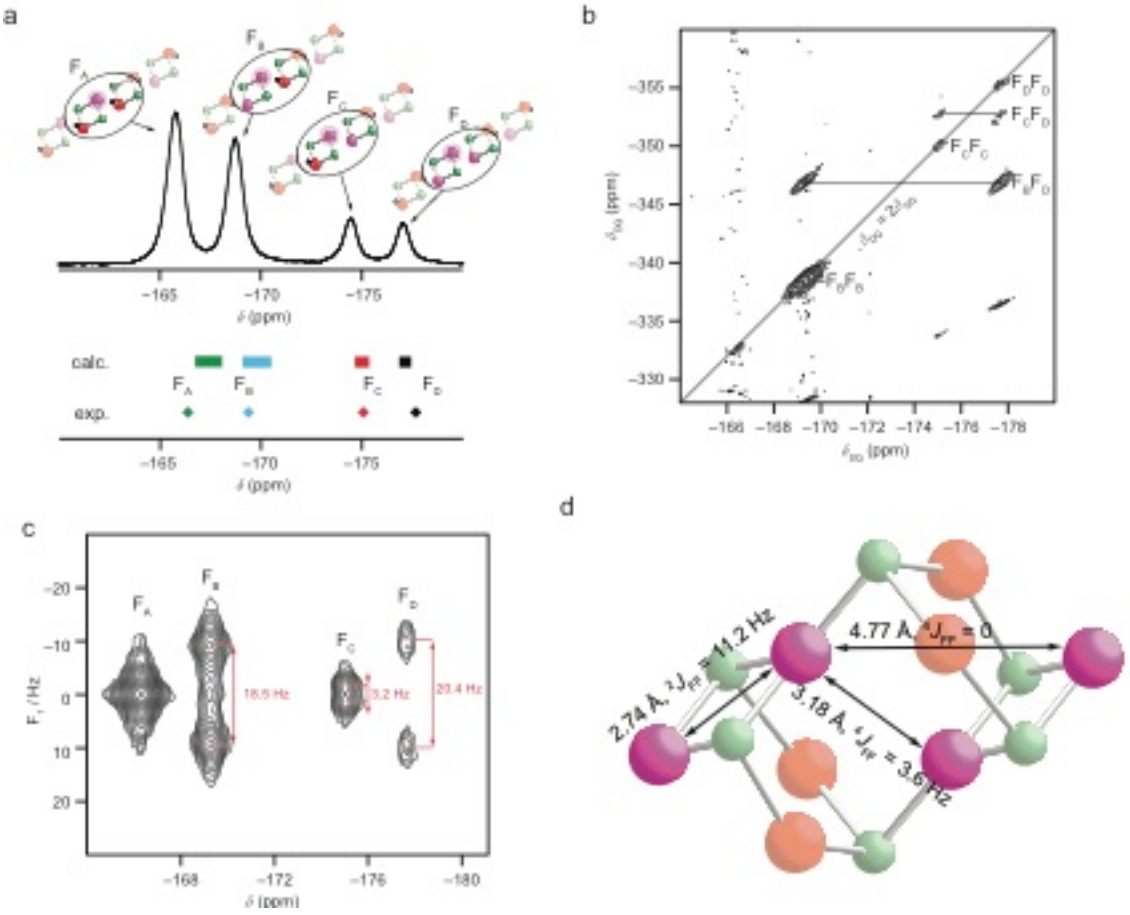
a
b
c
d
calc.
exp.
δ (ppm)
4.77 Å, $^4J_{FF}$ = 0
2.74 Å, $^2J_{FF}$ = 11.2 Hz
3.18 Å, $^4J_{FF}$ = 3.6 Hz

Conspectus

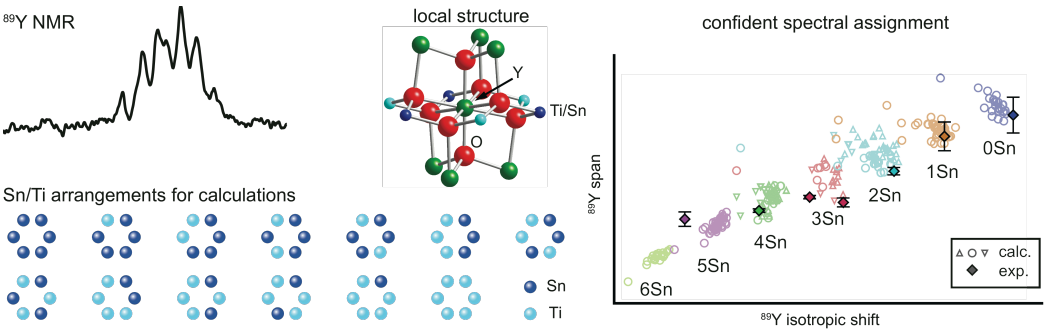
^{89}Y NMR
local structure
Y
O
Ti/Sn
Sn/Ti arrangements for calculations
Sn
Ti
confident spectral assignment
^{89}Y span
^{89}Y isotropic shift
6Sn
5Sn
4Sn
3Sn
2Sn
1Sn
0Sn
calc.
exp.